Impact of dynamic stall model tailoring on wind turbine loads and performance prediction

Chellini, Simone; De Tavenier, Delphine; Von Terzi, Dominic

DOI
10.1088/1742-6596/2767/2/022016

Publication date
2024

Document Version
Final published version

Published in
Journal of Physics: Conference Series

Impact of dynamic stall model tailoring on wind turbine loads and performance prediction

Journal of Physics: Conference Series **2767** (2024) 022016 doi:10.1088/1742-6596/2767/2/022016

Impact of dynamic stall model tailoring on wind turbine loads and performance prediction

Simone Chellini, Delphine De Tavenier, Dominic von Terzi
Delft University of Technology, Kluyerweg 1, 2629 HS Delft, The Netherlands
E-mail: s.chellini@tudelft.nl

Abstract. The future of wind turbines will be characterised by long, slender blades subject to dynamic inflow and aeroelastic deflections. This makes the next generation of blades more prone to encounter dynamic stall effects, in which significant forces and loads fluctuations can be expected. Dynamic stall models can be tailored to suit the aerodynamics of different airfoils. Although different dynamic stall models exist, the impact of the choice of model, its implementation and calibration on the overall wind turbine performance remains to be assessed. In this work, we gathered an experimental dynamic dataset for a representative airfoil, the FFA-W3-211, to define the semi-empirical time constants for the Beddoes-Leishman dynamic stall model. An important differentiation is made between stall regions for positive and negative angles of attack, and the impact of tailored coefficients is assessed at airfoil scale. The difference between the tailored and untailored model is quantified for power performance and loads of the IEA 15 MW reference wind turbine. The results highlight a significant load over-prediction from the untailored Beddoes-Leishman model, whereas changes in power performance are negligible.

1. Introduction

The current climate crisis is challenging the energy industry to accelerate energy production from renewable sources [1]. National governments and international organisations set ambitious targets, such as achieving 100% Green Energy by 2050 in the Netherlands. Wind energy plays a key role in achieving these goals. The next generation of *horizontal axis wind turbines* (HAWTs) will introduce the largest-ever rotors, with longer and more flexible blades. Large HAWTs are more prone to experiencing time-varying inflow conditions along the blades due to wind shear, turbulence, aeroelastic deflection and rotor misalignment [2]. This motivates studying the dynamic stall phenomena and its associated loading in this work.

Dynamic stall can be described as a phenomenon in which the boundary layer of an airfoil separates and reattaches due to a time-dependent change in angle of attack caused, for example, by a pitching motion or a gust. Flow reversal occurs in the boundary layer after the airfoil first exceeds the static stall angle. Depending on the airfoil, this is followed by a *leading edge vortex* (LEV) that energises the airfoil's boundary layer on the suction side and accounts for extra lift past the static stall angle. The maximum lift is achieved when the vortex reaches the leading edge. After this, stall is initiated from the leading or the trailing edge, depending on the inflow conditions and airfoil shape. Finally, the boundary layer reattaches on the suction side as the angle of attack decreases. The dynamic stall loop is characterised by a delay in boundary layer separation, an increase in C_{lmax}, a delay of the angle of attack at which this takes place and a higher drag coefficient for the separated flow region. A successful blade design must consider the

effects of dynamic stall on aeroelastic stability. To account for dynamic stall effects on airfoils and blades, many examples of dynamic stall modelling exist in the literature for different airfoils and applications [3]. Additionally, many experiments have obtained the empirical polars for pitched airfoils, such as [4], and used the empirical data to calibrate dynamic stall models [5]. While dynamic stall is found in many applications, dedicated literature exists for wind turbines, distinguishing between airfoil and blade level. In [6], a differentiation is made at the blade level, distinguishing between slow and fast regimes. The modelling work in [7] compares a newly generated model to traditional models, such as Beddoes-Leishman and Onera, showing good agreement and demonstrating that most camber effects are accounted for in the static input.

Reference wind turbines are standard research benchmarks. These publicly available designs allow researchers to build knowledge of wind turbines and wind farms starting from a shared baseline. One of the largest available, the IEA 15 MW [8], employs airfoils from the FFA family. The tip airfoil, the *FFA-W3-211*, covers the last 23% of the blade length and is, therefore, the airfoil subject to the highest loads on the blade. This work aims to calibrate the Beddoes-Leishman (BL) dynamic stall model with newly acquired data from a wind tunnel experiment, first solving the problem at the airfoil scale. The impact of the tailored and non-tailored model is determined at turbine scale through OpenFAST simulations.

2. Metholodogy

2.1. Experimental setup

An experimental campaign is carried out in the *Low-Speed Low-Turbulence wind tunnel* (LTT) at Delft University of Technology, a closed-section recirculating wind tunnel. The facility features changeable octagonal testing sections, with a width of 1.80m, length of 2.60m and height of 1.25m. The turbulence level varies from 0.015% at $20m/s$ to 0.07% at $75m/s$ due to the large contraction ratio of 17.8. An FFA-W3-211 airfoil model with a chord of $c = 600mm$ and a height of $h = 1246mm$ is built from carbon fibre composites (Figures 1 and 2). The model is equipped with 93 pressure ports on its surface, and a pressure rake is used to capture the loss of momentum in the wake. Firstly, a static dataset was acquired for Reynolds numbers in the range $5 \times 10^5 \leq R_e \leq 3.5 \times 10^6$. The airfoil polars were first validated against experimental and numerical results in Figure 3. The calibration was followed by a dynamic polars acquisition, for positive and negative *mean* angles of attack ($\alpha_0 = -8°, 0°, 11°$). Dynamic data was acquired for 50 cycles for chord-based Reynolds numbers of $R_{e_c} = 5 \times 10^5, 10^6, 2 \times 10^6$. However, only the dataset for $R_e = 10^6$ will be shown in this work. The airfoil was pitched around its quarter chord point through a linear actuator controlled by a LabVIEW interface, as defined in Equation 1:

$$\alpha(t) = \alpha_0 + Asin(2\pi ft), \tag{1}$$

where α_0 is the mean angle of attack, A is the amplitude of the oscillation, and f is the frequency. A reduced frequency $k = \pi fc/U_\infty$ describes the degree of unsteadiness. The unsteady effects can be neglected in the quasi-steady regime for $0 < k < 0.05$. The flow is considered unsteady for $0.05 \leq k < 0.2$; finally, for $k \geq 0.2$, the flow is considered highly unsteady [9]. Due to experimental constraints, the reference Reynolds number for the presented work will be fixed to $R_e = 10^6$, and only the normal coefficient will be discussed at airfoil level. Finally, retrieving the drag coefficient for the pitching airfoil case was impossible as the wake rake could not capture the large turbulent wake of the airfoil.

2.2. Corrections

The static polars are traditionally corrected for wake blockage, streamline curvature and compressibility effects as described in [10]. This allows to take into account quantifiable losses in 2D airfoil testing. Traditional dynamic data corrections are described in [11], accounting for

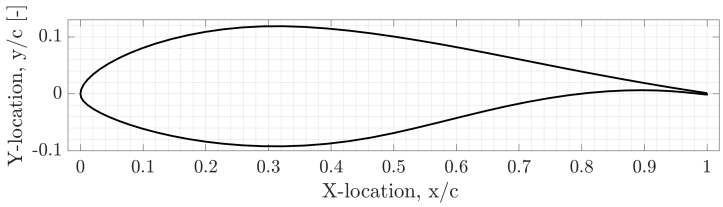

Figure 1. Cross section of the FFA-W3-211 airfoil.

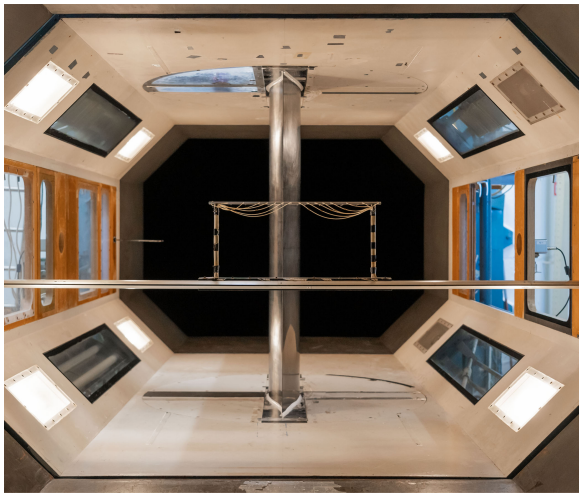

Figure 2. The octagonal LTT testing section with the wake rake and the airfoil model set to $AoA = 0°$. View from downstream of the trailing edge.

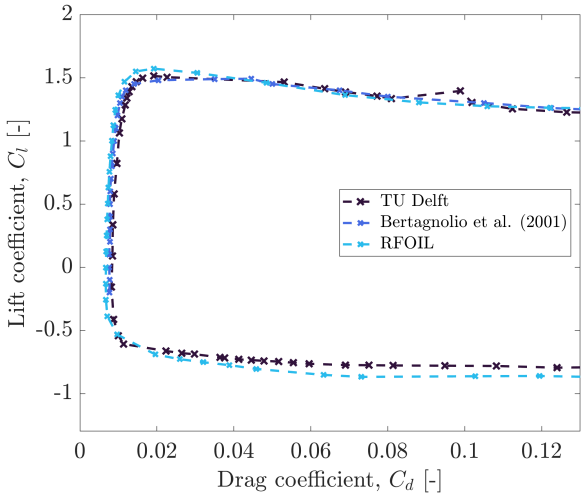

Figure 3. Validation plot for experimental data against data from Bertagnolio [12] and RFOIL [13] results for $R_e = 1.8 \times 10^6$.

the pressure lag between the airfoil's skin and the data acquisition reading. Static and dynamic polars correction decision greatly affects the Beddoes-Leishman calibration results. Figure 4 shows the corrected, uncorrected and partially corrected lift curve slope. The partially corrected plot shows the same corrections from [10] implemented without the drag coefficient term, which could not be retrieved for the dynamic case. As expected, the effects of wake blockage become more significant at high angles of attack. The effects of static corrections on the Beddoes-Leishman method are examined in Figure 5. The default time coefficients from OpenFAST are used (Table 1), and the curve is generated for the corrected and uncorrected input. Simulation can be compared against experimental results, corrected only for the acquisition time delay and divided between upstroke (full line) and downstroke (dotted line). Despite a greater relative error between the experimental results and uncorrected dynamic stall results, it was decided to use the uncorrected polars as input for the Beddoes-Leishman model as the static correction would be dependent on the angle of attack, which varies in the BL-hysteresis.

2.3. Beddoes-Leishman model

To assess the dynamic stall impact at turbine scale, the semi-empirical iterative model developed by Beddoes and Leishman [2] is tailored to the FFA-W3-211 results. The model is divided into attached flow, separated flow (leading and trailing edge separation) and dynamic stall (vortex shedding) modules. This module division can be used to determine the contributions from the different phases of dynamic stall. The original model was validated with dynamic experiments

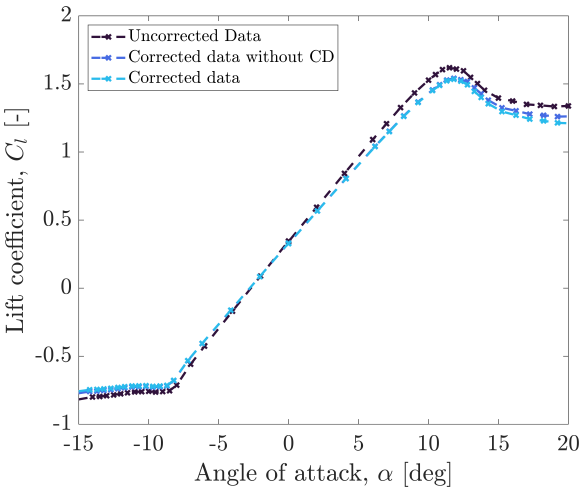

Figure 4. Effects of static corrections from [10] on the lift curve slope for a clean airfoil at $R_e = 10^6$ on the experimental data.

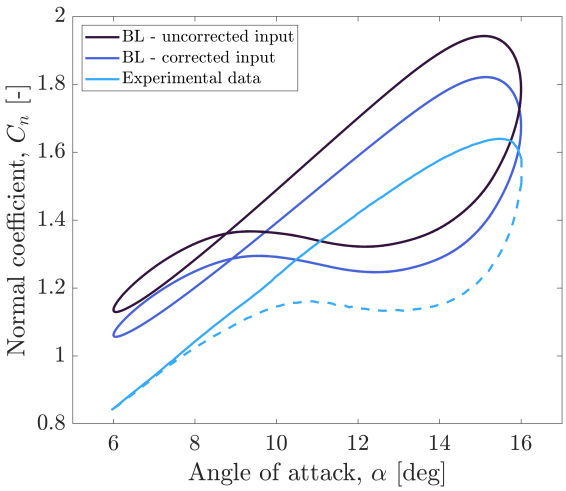

Figure 5. Initial hysteresis loops for corrected and uncorrected polars input for $R_e = 10^6$, compared against experimental data for $a_0 = 11°$, $A = \pm 5°$, $f = 1.2Hz$ (k = 0.091).

for a NACA0012 airfoil with $R_{e_c} = 8 \times 10^6$ and $M = 0.4$. The BL model has been widely used and edited in the literature due to its flexibility in modelling dynamic stall, as only the lift and drag coefficient and the angle of attack are needed as input to obtain the equivalent dynamic loads on an airfoil. The model uses four coefficients (A1, A2, B1, B2), derived from thin airfoil theory, and four time-delay constants, which describe the time delay in the aerodynamic loading. This study aims to determine the optimal time-delay constants for the FFA-W3-211 airfoil:

- T_p is the pressure lag time constant. It is a Mach number dependent, but largely shape independent, parameter that must be derived from dynamic data [2].
- T_{vl} is the vortex shedding time coefficient representing the time it takes for the leading edge vortex to shed over the airfoil. Due to the added vorticity, the coefficient can be assumed as a time of maximum aerodynamic loading [5].
- T_f is the viscous lag. It is a Mach number and airfoil shape dependent time constant.
- T_v is the vortex lift time constant. Similarly to T_p, it mainly depends on the Mach number and not so much on the airfoil shape [14].
- T_l is the non-circulatory time constant, defined as the ratio between the airfoil's chord and sonic speed.
- K_α is a factor associated with the non-circulatory time constant, dependent on the Mach number. As $M \to 0$, $K_\alpha \to 0.75$.

Some coefficients can be trivially derived, such as T_l and K_α. Others must be obtained from experimental data. All the parameters can be non-dimensionalised.

2.4. OpenFAST environment

OpenFAST is a multi-physics open-source tool that allows for aero-servo-elastic simulations of wind turbines to be performed with various support structures [16]. The IEA 15 MW is currently the largest reference wind turbine available, with a 22 MW turbine under development. Both designs employ airfoils from the FFA family, with the FFA-W3-211 representing the blade's

tip. Depending on the release, the OpenFAST environment features different built-in versions of different dynamic stall models, which can be deactivated or customised. In this work, we used the v3.5.0 version [17], tailoring the baseline Beddoes-Leishman model in the AeroDyn15 module, as described in [2]. The parameters relative to dynamic stall models can be changed at the airfoil level. A set of default parameters for the BL model is found in Table 1. The IEA 15 MW reference wind turbine features a rotor radius of $120m$, a maximum tip speed of $95ms^{-1}$ and operates in a wind regime between 3 and 25 ms^{-1}, with a rated speed of $U_\infty = 10.59ms^{-1}$ [15].

3. Results

3.1. Beddoes-Leishman parameters - Airfoil scale

The dynamic pressure lag can be found from dynamic experimental data as suggested in [18] by determining and averaging the angle of attack at which the normal coefficient is the highest for each oscillation. Results in Figure 6 show the scattered plot for a range of oscillating motions, for amplitudes of $A = 3°, 5°, 7°, 9°, 11°$, frequencies of $0.6, 1.2, 1.8, 2.4Hz$, and a mean angle of attack of $\alpha_0 = 11°$. Here, the few cases with no boundary layer separation were excluded from the analysis. A reduced pitch describing a ramp-up motion as

$$r = \frac{\dot{\alpha} c}{U_\infty}, \tag{2}$$

where $\dot{\alpha}$ is the maximum pitch-rate, obtained by taking the time derivative of Equation 1 yielding $\dot{\alpha} = 2\pi f A \cos(2\pi f t)$.

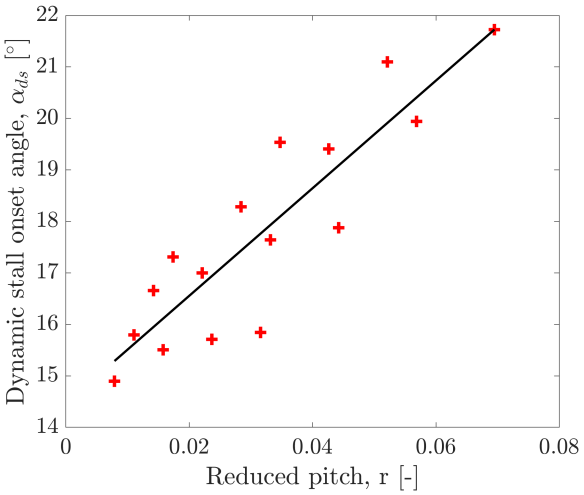

Figure 6. Scattered and fit results from the dynamic stall onset for $R_e = 10^6$ for the positive region of the polars ($\alpha_0 = 11°$).

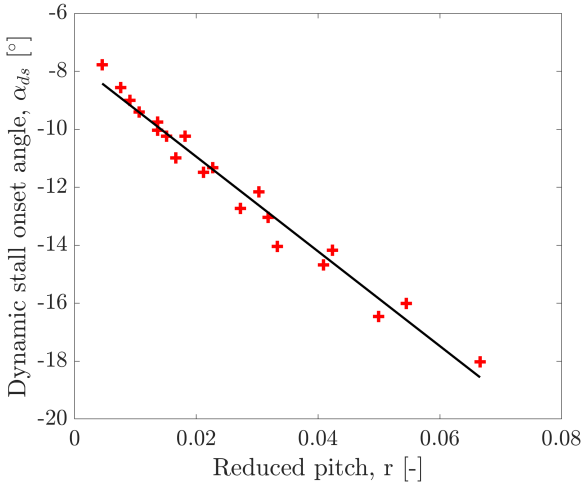

Figure 7. Scattered and fit results from the dynamic stall onset for $R_e = 10^6$ for the negative region of the polars ($\alpha_0 = -8°$).

The slope in Figure 6 returns a pressure lag of $T_p = 1.92s^{-1}$ for the positive stall regime. As expected, the dynamic stall onset greatly depends on the Reynolds number, increasing for higher values. As a comparison, the pressure lag changes to $T_p = 0.79$ for $R_e = 5 \times 10^5$, and to $T_p = 2.78$ for $R_e = 2 \times 10^6$. Furthermore, a higher Reynolds number increases the accuracy of the slope prediction and reduces the data scatter. The same methodology is used for the negative stall angle. The absolute value of the slope shown in Figure 7 leads to $T_p = 2.85s^{-1}$, showing a lower standard deviation.

In [19], different approaches are presented to determine the vortex-shedding time-coefficient T_{vl}. Similarly to T_p, the coefficient varies greatly depending on the oscillating frequency of the wing. If the full flow field cannot be reconstructed from PIV or numerical data, the coefficient can be retrieved from the pressure distribution around the suction side of the airfoil or interpolated numerically. A local minima in the pressure distribution on the suction side detects the vortex velocity travelling from the leading edge to the trailing edge. Alternatively, the position of the vortex can be inferred from the measured unsteady loads, computing the dynamic-stall onset time and the time of maximum aerodynamic loading, as seen in Figure 8. This last method was used to determine the vortex-shedding time for a mean angle of $\alpha_0 = -8°$, as the leading edge vortex was detected for some of the negative mean angle cases only. The vortex-shedding time was normalised by the ratio between the free-stream velocity and the airfoil's chord as $T_{vl} = t_{vl}U_\infty/c$ and is shown in Figure 9. The high data scatter suggests that the delay of leading-edge vortices is greater at lower reduced pitches, in agreement with results in [19].

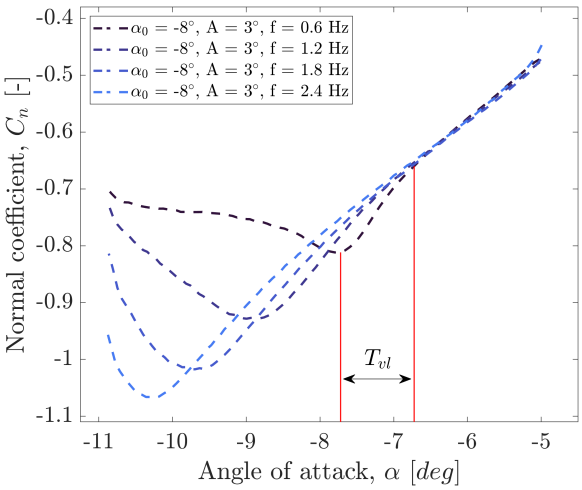

Figure 8. Downstroke normal coefficient for $\alpha_0 = -8°$, $A = \pm 3°$ highlighting the vortex-shedding time-delay for $f = 0.6Hz$.

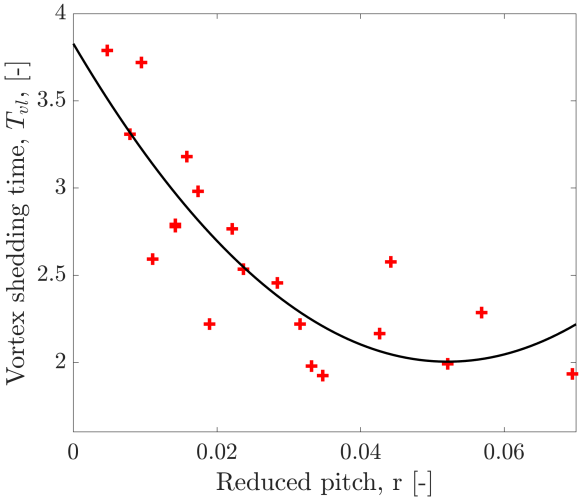

Figure 9. Vortex-shedding time vs. reduced pitch-rate for $\alpha_0 = -8°$, $R_e = 10^6$. The interpolation is carried out with a second order fit, as seen in [5].

Due to the cambered geometry of the FFA airfoil, the characteristic local pressure minima on the suction side were not observed in our data for positive mean angles of attack. Furthermore, the normal coefficient slope deflection was not reached before the C_n peak, suggesting no significant effect induced by the shedding of the leading edge vortex. This can be seen in Figure 5 and Figure 11, where an almost uniform slope is found from the experimental data. Therefore, it was decided to keep the value of $T_{vl} = 6$ for positive mean angles of attack.
The Swedish FFA [20] validated the Beddoes-Leishman model for several thick airfoils for wind turbines for unsteady reduced frequencies. The LS(I) 0421 MOD airfoil offers similar characteristics to the FFA-W3-211, such as camber and maximum thickness, and allows the determination of the remaining two time coefficients as $T_f = 6.95$ and $T_v = 0.89$. Table 1 shows the final list of time coefficients.

The impact of the coefficients shown in Table 1 on the airfoil dynamic polars is evaluated using the original version of the Beddoes-Leishman code, computing the normal coefficient for a range of representative angles of attack, reduced frequencies and amplitudes. Initially, the difference shown in Figure 5 is due to factors such as three-dimensional flow effects, dynamic correction

Table 1. Optimal time coefficients for the FFA-W3-211 for $R_e = 10^6$.

	A_1	A_2	B_1	B_2	T_f	T_v	T_p	T_{vl}
OpenFAST default parameters	3.0	6.0	1.7	11	3.0	6.0	1.7	11
Positive mean angles of attack	3.0	6.0	1.7	11	6.95	0.89	1.92	6
Negative mean angles of attack	3.0	6.0	1.7	11	6.95	0.89	2.85	2.55

and experimental uncertainty. The uncorrected normal coefficient curve was normalised by its relative maximum to compare the shape of the Beddoes-Leishman hysteresis loop and assess how the new parameters set describes different hysteresis phases. Thus, the difference in normal coefficient between the experimental results and the BL-model iterations can be defined as Equation 3:

$$\varepsilon = \frac{1}{N}\sum_{i=1}^{N}\left|\frac{C_{N_{E,i}} - C_{N_{BL,i}}}{C_{N_{E,i}}}\right| \tag{3}$$

where the denominator indicates the experimental values. The relative error of the normalised and optimised results for positive mean angles of attack leads to $\varepsilon_{optimal} = 1.48\%$ for the oscillating parameters in Figure 11. This is over 0.5% lower than the error between the experimental and the non-optimised Beddoes-Leishman model ($\varepsilon_{OpenFAST} = 2.06\%$). While the experimental optimisation improves the normal coefficient prediction compared to the experimental data, the newly found coefficients also allow us to better predict the hysteresis at low angles of attack. The original BL-model presented an exaggeration in the initial loop, showing significant differences between the upstroke and downstroke phases. Finally, the nose-down reattachment also shows some significant differences, with the optimised time-coefficients underestimating the boundary layer reattachment mechanisms on the suction side of the airfoil, leading to a lower performance.

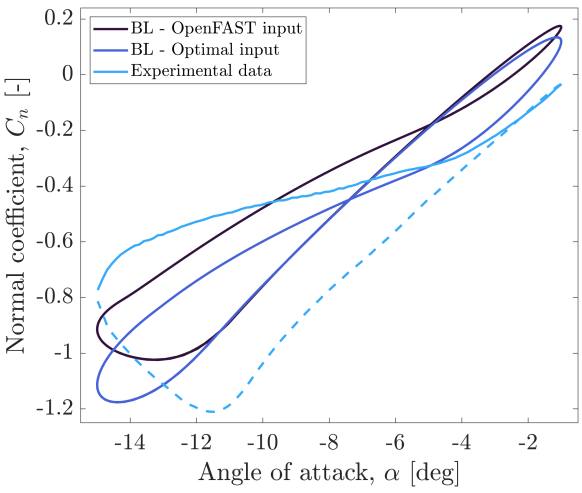

Figure 10. Normal coefficient hysteresis loops for $R_e = 10^6$, $a_0 = -8°$, $A = \pm 7°$, $f = 1.2Hz$ (k = 0.091).

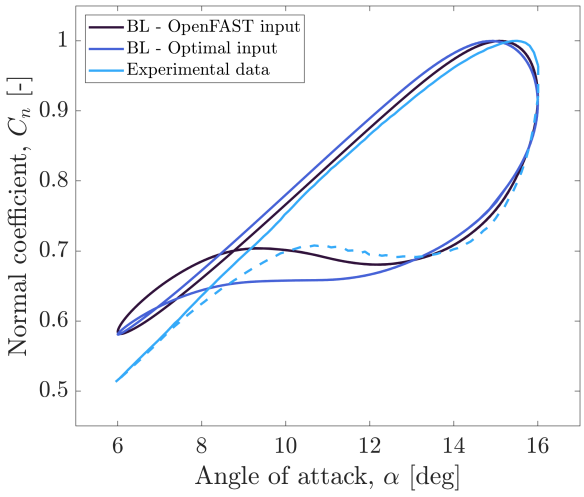

Figure 11. Normalised normal coefficient hysteresis loops for $R_e = 10^6$, $a_0 = 11°$, $A = \pm 5°$, $f = 1.2Hz$ (k = 0.091).

The mean negative angle results show greater differences between the non-optimised and optimised BL-models against experimental results. Unlike the positive mean region, the difference is also observed to depend on the amplitude of oscillation and the frequency. Results are shown in Figure 10, for the non-normalised normal coefficient. Here, the optimised input improves the dynamic stall prediction for the downstroke oscillation, and mildly displays the effect of the leading edge vortex shed over the suction side of the airfoil. The optimisation results also better replicate the minimum normal coefficient obtained at the beginning of the pitching motion. However, the optimised results overpredict the hysteresis loop at the highest angles of attack, which is not found in the experimental data, and only marginally in the non-optimised BL-model.

3.2. IEA 15 MW performance - Turbine scale

The tailored coefficients from Table 1 were imported in OpenFAST, but only for the FFA-W3-211 airfoil. This covers approximately the last 23% of the IEA 15 MW blade. The monopile configuration of the IEA 15 MW was used, which can reach chord-based Reynolds numbers of up to $R_e = 1.5 \times 10^7$. A turbulent input was generated with the Turbsim tool, a stochastic full-field turbulent flow simulator, replicating an IECKAI model with category 1A and 3C wind classes and turbulence levels. The reference height was kept to default as $168m$, with a mean wind-speed of $U_\infty = 9$ and $18ms^{-1}$. The analysis here focuses on the below-rated regime for a blade pitch angle of zero degrees for the same rotor speed. The OpenFAST v3.5.0 BL model implementation is found in [21] and uses C_n and C_c as inputs, coupled with the set of time-delay coefficients described in the original Beddoes-Leishman model [2].

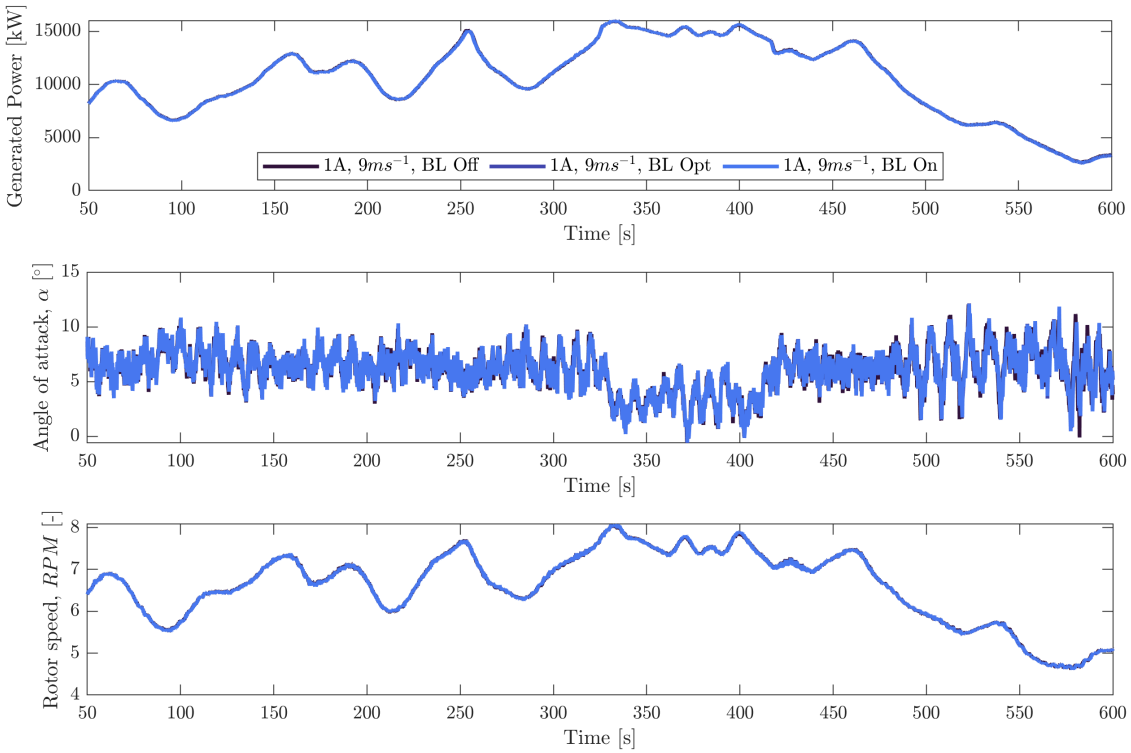

Figure 12. Turbine results for turbulent wind (class 1A), $U_\infty = 9ms^{-1}$: power output (top), angle of attack (centre) and rotor speed (bottom) for node 43 on the IEA 15 MW blade.

Three simulations were carried out for the positive AoA region of the polars to assess the impact of the absent, tailored and untailored dynamic stall model, for which ten seeds were used for each case for an individual run time of 600 seconds. Results for the 1A wind class are illustrated in Figure 12. When both dynamic stall models are turned off, the power output is over-predicted by 0.33%. The non-tailored BL-model shows a power output over-prediction over the tailored model by 0.013% with respect to the tuned model. Similar trends are found for the lower turbulence intensity case, for the same wind class. Despite not reaching the dynamic-stall angle-of-attack region, valuable results are observed in the local AoA variation. These results show an over-prediction of the local airfoil AoA from the untailored Beddoes-Leishman model of up to one degree during fast transients. Finally, the non-tailored BL model over-predicts the maximum aerodynamic loads across the blade span, for instantaneous values up to $1kN$ during fast transients.

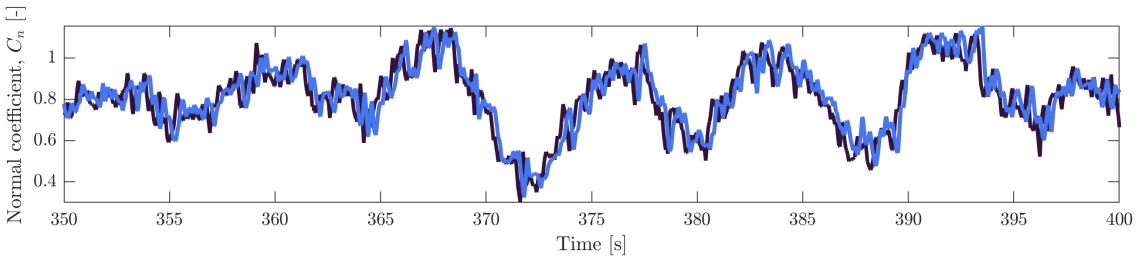

Figure 13. Normal coefficient variation for node 43 on the IEA 15 MW blade.

Looking at the local normal-coefficient variation, the untailored dynamic-stall model overestimates the 2D airfoil coefficient (Figure 13). Despite the slight phase shift, the tailored Beddoes-Leishman model shows a better agreement with the reference data in which no dynamic-stall model is used, showing different local maxima and minima points. The results suggest that appropriate time coefficients should be used for each airfoil. While this work aimed to verify the turbine performance depending on the dynamic-stall time variable used, it was only possible to edit one airfoil in the IEA 15 MW, covering the last $\approx 23\%$ of each blade. In OpenFAST, the same set of coefficients is used for all the airfoils employed in the design, leading to a mismatch in terms of aerodynamic loading.

4. Conclusions and future work

Large wind turbines are more prone to suffer the consequences of strong dynamic inflow. This work evaluated the impact of tailoring the coefficients of the Beddoes-Leishman dynamic-stall model for a wind-turbine tip airfoil on turbine performance and blade loading. An experimental dynamic dataset has been gathered for the first time for the FFA-W3-211 airfoil, pitching for a range of reduced frequencies, amplitudes and mean angles-of-attack.

The data was used to determine the relevant dynamic-stall time-coefficients in the Beddoes-Leishman model, highlighting important differences between the positive and negative stall regimes. At the airfoil scale, the performance improvement of the tailored BL-model against the non-tailored BL-model was quantified as 0.5%, i.e. a ca. 25% error reduction, with substantial gains in matching the hysteresis-loop shape. The negative regime optimisation improved results over the non-tailored BL-model for some aspects, but still fails to replicate the dynamic behaviour of the FFA-W3-211 airfoil.

At turbine level, significant differences were found. Despite not reaching the equivalent dynamic-stall angle, the original BL-model returns higher airfoil loads and angles-of-attack than the tailored variant. Additionally, the IEA 15 MW floating version will likely encounter even

more severe load variations due to a more dynamic inflow.

Finally, the experimental finding that the dynamic stall behavior at positive and negative AoA is significantly different (compare Figures 10 and 11) suggests that these regimes may benefit from being tuned or even modeled differently in wind turbine simulations. The reason for this is that, during normal wind turbine operations, the positive angles are more likely encountered at below rated conditions and are more critical for power performance predictions, whereas the negative AoA regime is more frequently experienced above rated and may be more design driving with respect to admissible loading. To this end, more research and improved modelling is needed.

References

[1] Veers P, Dykes K, Lantz E, Barth S, Bottasso CL, Carlson O, Clifton A, Green J, Green P, Holttinen H, Laird D., 2019. Grand challenges in the science of wind energy. *Science* 25.
[2] Leishman JG, Beddoes TS, 1989. A Semi-Empirical model for dynamic stall. *Journal of the American Helicopter Society* 34(3), pp. 3–17.
[3] Leishman JG. Challenges in modelling the unsteady aerodynamics of wind turbines, 2002. *Wind Energy* 5(2-3), pp. 85–132.
[4] McCroskey WJ, McAlister KW, Carr LW, Pucci SL, 1982. An experimental study of dynamic stall on advanced airfoil sections. Volume 1: Summary of the experiment. *NASA Technical Memorandum* 84245.
[5] Sanchez Martinez M, Boutet J, Amandolese X, Terrapon V, Dimitriadis G., 2019. Computation of Leishman-Beddoes model parameters using unsteady RANS simulations. In *AIAA SciTech 2019 Forum and Exhibition.*
[6] Santos Pereira R. Aerofoil Aerodynamics of Wind Energy Devices. Handbook of Wind Energy Aerodynamics. 2020:1-22.
[7] Larsen JW, Nielsen SR, Krenk S. Dynamic stall model for wind turbine airfoils. Journal of Fluids and Structures. 2007 Oct 1;23(7):959-82.
[8] Gaertner E, Rinker J, Sethuraman L, Zahle F, Anderson B, Barter G, Abbas N, Meng F, Bortolotti P, Skrzypinski W, Scott G, 2020. Definition of the IEA 15-megawatt offshore reference wind turbine. *National Renewable Energy Laboratory.* NREL/TP-5000-75698.
[9] Corke TC, Thomas FO, 2015. Dynamic stall in pitching airfoils: aerodynamic damping and compressibility effects. *Annual Review of Fluid Mechanics* 3;47, pp. 479–505.
[10] Dalton C, 1971. Allen and Vincenti blockage corrections in a wind tunnel. *AIAA Journal* 9(9), pp. 1864–5.
[11] De Tavernier D, Ferreira C, Viré A, LeBlanc B, Bernardy S, 2021. Controlling dynamic stall using vortex generators on a wind turbine airfoil. *Renewable Energy* 1;172, pp. 1194–211.
[12] Bertagnolio F, Sørensen N, Johansen J, Fuglsang P, (2001). Wind turbine airfoil catalogue. *Risøe report* 1280.
[13] Van Rooij RP, 1996. Modification of the boundary layer calculation in RFOIL for improved airfoil stall prediction. *TU Delft Wind Energy Technical Report* IW-96087R.
[14] Pereira R, Schepers G, Pavel MD, 2012. Validation of the Beddoes–Leishman dynamic stall model for horizontal axis wind turbines using MEXICO data. *Wind Energy* 16(2), pp. 207–19.
[15] De Tavernier D, Von Terzi D, 2022. The emergence of supersonic flow on wind turbines. In *Journal of Physics: Conference Series* 2265 (4), pp. 042068).
[16] National Renewable Energy Laboratory Openfast v3.5.0 https://github.com/openfast/openfast/ online; Accessed on 04-03-2024
[17] OpenFASt User Documentation. Unsteady Aerodynamics https://openfast.readthedocs.io/en/main/source/user/aerodyn/theoryua.html online; Accessed on 04-03-2024
[18] Sheng W, Galbraith RM, Coton FN, 2008. Prediction of dynamic stall onset for oscillatory low-speed airfoils. *Journal of Fluids Engineering* 130(10).
[19] Boutet J, Dimitriadis G, Amandolese X, 2020. A modified Leishman–Beddoes model for airfoil sections undergoing dynamic stall at low Reynolds numbers. *Journal of Fluids and Structures* 1;93:102852.
[20] Mert M, 1999. Optimization of semi-empirical parameters in the FFA-Beddoes dynamic stall model. *FFA-TN-1999-37.*
[21] Damiani RR, Hayman G, 2019. The unsteady aerodynamics module for fast8. *National Renewable Energy Lab (NREL)*, Golden, CO (United States).